

# Sheets and Filaments as the Origin of the High-Velocity Tail of the Ly $\alpha$ Forest

Robert E. Rutledge

Max-Planck-Institut für Extraterrestrische Physik, Postfach 1603, D-85740 Garching,  
Germany

rutledge@rosat.mpe-garching.mpg.de

## ABSTRACT

Simulations of large-scale structure formation predict the formation of sheet- and filamentary structures, which are often invoked as the origin of the Ly $\alpha$  forest. In their simplest description, these sheets and filaments require a differential distribution of observed line-of-sight velocity widths ( $b$ ) which will decrease as power-laws at velocities well above the observed peak in this distribution: for filaments, the differential distribution is  $dN/db \propto b^{-3}$ , while for sheets it is  $dN/db \propto b^{-2}$ . These functional dependences on  $b$  arise *a priori* due to the geometry of these absorbing structures – assuming random orientations relative to the line-of-sight – and are otherwise unrelated to the physical state in the absorbing structure. We find the the distribution at  $b > 35$  in three previously published data sets to be steeper than  $dN/dB \propto b^{-3}$  (99.99% confidence). This implies that evidence of the finite length of these kinds of absorbing structures is present in the  $b$ -distribution data.

*Subject headings:* cosmology: early universe — cosmology: intergalactic medium — galaxies: quasars: absorption lines

## 1. Introduction

The observational distribution of measured velocity widths ( $b$ ) of Ly $\alpha$  forest absorption lines may be parameterized as Gaussian, but with a significant non-Gaussian, high-velocity tail ( $\geq 55$  km sec $^{-1}$ ; cf. Hu et al. 1995; Lu et al. 1996; Kim et al. 1997; Kirkman & Tytler 1997; Khare et al. 1997 for recent observational results).

Investigations based on spherical gaseous clouds bounded by external pressure (Duncan et al. 1991; Petitjean et al. 1993) find that the  $b$ -distribution can only be reproduced by a population with a strong correlation between central density, radii, and cloud mass, requiring a tight correlation between column density and  $b$ , which has not been strongly supported by the data (Rauch et al. 1993, discusses selection effects which may have produced earlier reported correlations). Other researchers find that high implied temperatures of such clouds (assuming  $b = \sqrt{2kT/m_p}$ ) cannot be produced by structures in thermal equilibrium with an ionizing UV background, and may imply recent adiabatic collapse (Press & Rybicki 1993).

The ramifications of CDM structure formation models as the origin of the Ly $\alpha$  forest have been extensively investigated. Recent workers, using hydrodynamic simulations of cosmological models (usually CDM or  $\Lambda$ CDM), describe the structures responsible for the low-density ( $N_H \lesssim 10^{15}$ ) Ly $\alpha$  forest to be filaments, pancakes, “cigar-like”, mini-pancakes, or sheets (Cen et al. 1994; Zhang et al. 1995; Hernquist et al. 1996; Katz et al. 1996; Miralda-Escudé et al. 1996; Bi & Davidsen 1997; Cen & Simcoe 1997; Nath 1997; Zhang et al. 1997). Commonly, the  $b$ -distribution is parameterized as a Gaussian; in addition, a non-Gaussian high-velocity tail is universally noted. The measured  $b$ -values do not always correspond directly to a temperature, and most structure formation theories produce fluctuations in the density of the inter-galactic medium (IGM) larger (in redshift space) than the thermal width (Miralda-Escudé et al. 1996; Hui et al. 1997).

In this *Letter*, we describe how this high-velocity tail may be generated by the same structures responsible for the lower-velocity Gaussian peak. The low-velocity (Gaussian peak) values are caused by the line-of-sight passing nearly perpendicular to the long-axis of the sheet/filament-type structures, while the high-velocity tail is due to higher angles of incidence. The relative number of low vs. high  $b$ -values are, in this scenario, determined by the geometry of the absorbing structures, and is otherwise unrelated to the physical state of the absorbing structure.

In exploring this scenario, we keep in mind the fact that the fluctuations which are produced in large-scale structure formation simulations are in a continuous density field, and ascribing a simplified geometry to them in the way we do (as a cylinder, or an infinite sheet) is an idealization of a structure which has already been observed in the simulations to be more complicated.

## 2. The Model: Line-of-Sight $b$ -Distribution

In this model, the magnitude of  $b$  corresponds to the line-of-sight width of the absorbing structure in velocity space, which is determined both by its physical size in comoving space and by its peculiar velocity structure.

### 2.1. Cylindrical Filaments

In the simplest manifestation (refer to Fig. 1), an observer’s line-of-sight (LOS) crosses an absorber which has a minimum (velocity) width  $b_0$ , and which has a long-axis. We assume that the geometry of the absorber is such that the cross section – which is the plane shared by the short-axis  $b_0$  and the LOS, parallel to the long axis – can be described as a rectangle of width  $b_0$  and quasi-infinite length. This is a fair assumption to describe cross-sections of filaments and sheets, but not of spheres. Presently, we treat the long-axis as infinite, but the expected finite length would produce observationally important effects, which we discuss below.

The LOS crosses the absorber at an angle  $\theta$  to the perpendicular of  $b_0$ , producing a line-of-sight crossing distance (in velocity space) of  $b$ . The observed velocity-width  $b$  is geometrically related to the short axis  $b_0$ :

$$b = \frac{b_0}{\sin(\theta)} \quad (1)$$

This is the relationship between the LOS velocity-width ( $b$ ) of the observed absorption line and the velocity-width  $b_0$  of the density enhancement (that is, filament or sheet). If we assume a random distribution in  $\theta$  (that is, a random orientation of absorbing structures relative to the LOS), because  $\theta = 0$  is the axis of symmetry for the cylindrical filament, the number of LOS per unit  $\theta$  is:

$$\frac{dN_{\text{cyl}}}{d\theta} = \sin(\theta) \quad (2)$$

and the number of LOS per unit velocity for a constant  $b_0$  – is:

$$\frac{dN_{\text{cyl}}}{db}(b, b_0) = \frac{dN}{d\theta} \frac{d\theta}{db} = \begin{cases} -\frac{\left(\frac{b_0}{b}\right)^3}{b_0 \sqrt{1 - \left(\frac{b_0}{b}\right)^2}} & b > b_0 \\ 0 & b \leq b_0 \end{cases} \quad (3)$$

We assume a cylindrical filament, with a diameter  $L$ ;  $b_0$  then depends on an angle  $\phi$ , corresponding to an impact parameter relative to the center of the cylinder's circular cross-section:

$$b_0 = L \cos(\phi) \quad (4)$$

where  $\phi = 0$  when the LOS passes through the center of the cylinder's circular cross-section, and  $\phi \approx \pi/2$  when the LOS passes nearly tangent to the cylinder's circular cross-section. The resulting distribution of  $b_0$ , assuming a random distribution of impact parameters, is:

$$\frac{dN}{db_0} = \frac{-\left(\frac{b_0}{L}\right)}{L\sqrt{1 - \left(\frac{b_0}{L}\right)^2}} \quad (5)$$

If we assume a random distribution of angles, the total  $b$ -distribution, using Eqn. 3, becomes

$$\frac{dN_{\text{cyl}}}{db}(b, L) = \frac{dN_{\text{cyl}}}{db}(b, b_0) \frac{dN}{db_0} db_0 = \frac{1}{L} \left(\frac{L}{b}\right)^3 \int_{\phi'}^{\frac{\pi}{2}} \frac{\cos^3(\phi)}{\sqrt{1 - \left(\frac{L}{b}\right)^2 \cos^2(\phi)}} d\phi \quad (6)$$

$$\phi' = \begin{cases} 0 & b > L \\ \arccos\left(\frac{b}{L}\right) & b < L \end{cases} \quad (7)$$

After making a change of variables of  $X = \sin(\phi)$ , converting the integrating variable from  $d\phi$  to  $d(\sin(\phi))$ , and replacing  $\frac{b}{L} = \mathcal{X}$ , the integral is in a tabulated form (Dwight 1961, 200.01 and 202.01). Once integrated, we find the distribution of velocity-widths  $b$  to be:

$$\frac{dN_{\text{cyl}}}{db}(b, L) = \begin{cases} \frac{1}{2L} \left[ \left(1 + \frac{1}{\mathcal{X}^2}\right) \ln\left(\frac{\mathcal{X}+1}{\sqrt{\mathcal{X}^2-1}}\right) - \frac{1}{\mathcal{X}} \right] & \mathcal{X} > 1 \\ \frac{1}{2L} \left[ \left(1 + \frac{1}{\mathcal{X}^2}\right) \ln\left(\frac{\mathcal{X}+1}{\sqrt{1-\mathcal{X}^2}}\right) - \frac{1}{\mathcal{X}} \right] & \mathcal{X} < 1 \end{cases} \quad (8)$$

This is the normalized  $b$ -distribution function for an ensemble of cylindrical filaments of velocity-diameter  $L$ , oriented randomly with respect to the line-of-sight. This distribution function is plotted in Fig. 2a, super-imposed on combined datasets 1+3+5 (see Table 1). The distribution is sharply peaked, with a broader wing at lower-velocities than at higher velocities. It is a very poor description of the data near the Gaussian peak, indicating that, at the very least, a distribution of  $L$  values must be imposed.

Expanding the logarithm in  $\mathcal{b}$  in Eq. 8, we find:

$$\frac{dN_{\text{cyl}}}{db}(b, L) \propto \frac{1}{\mathcal{b}^3} + \frac{1}{O(b^5)} + \dots \quad \mathcal{b} > 1 \quad (9)$$

plus higher order terms. Thus, the differential distribution of LOS velocities at values greater than the velocity diameter of the cylinder decreases as an inverse cube of the measured velocity. Because this decrease is a power-law, integrating over a distribution in  $L$  will not change it's power-law nature at  $b > L_{\text{max}}$  (where  $L_{\text{max}}$  is the largest contributing  $L$  value).

The differential distribution can be integrated, producing the the normalized cumulative distribution:

$$N_{\text{cyl}}(> b; b, L) = \begin{cases} \frac{1}{2}(1.0 - (\mathcal{b} - \frac{1}{\mathcal{b}}) \coth^{-1}(\mathcal{b})) & \mathcal{b} > 1 \\ \frac{1}{2}(1.0 - (\mathcal{b} - \frac{1}{\mathcal{b}}) \tanh^{-1}(\mathcal{b})) & \mathcal{b} < 1 \end{cases} \quad (10)$$

which is the fraction of  $b$  values expected to be larger than some value  $b$ , for a known value of  $L$ . The median is  $\mathcal{b} = 1.0$  (that is,  $b = L$ ). Approximately eighty per cent of the  $b$  values are between 0.5 and 2.0 of the median. At the high velocity end ( $\mathcal{b} \gg 1$ ), the cumulative  $b$ -distribution decreases as  $\mathcal{b}^{-2}$ , as expected. We show this cumulative distribution for an assumed  $L = 28 \text{ km sec}^{-1}$ , super-imposed on datasets 1+3+5 (see Table 1), in Fig. 2b. The power-nature of the cumulative distribution at  $b > 28 \text{ km sec}^{-1}$  is apparent, and is comparable to that seen in the dataset. (We comment on the possibility of a break in the data near  $b = 80 \text{ km sec}^{-1}$  in Sec 3, where we statistically compare the observed distribution with a power-law distribution).

## 2.2. Sheets

The differential distribution for sheets may be found similarly to cylinders. The relationship between  $b$  and  $b_0$  (the short axis velocity) is as in Eq. 1, where again we refer to Fig. 1. However, the axis of symmetry for the sheet is now perpendicular to the surface of the sheet, and the number of LOS per angle  $\theta$  changes accordingly (compare with Eq. 2):

$$\frac{dN_{\text{sheet}}}{d\theta} = \cos(\theta) \quad (11)$$

This is the important difference with the filament distribution. We assume a delta-function distribution of  $b_0 (=L - \text{the width of the sheet})$ . By chain rule, the differential  $b$ -distribution is:

$$\frac{dN_{\text{sheet}}}{db}(b, L) = \begin{cases} \frac{1}{L} \left(\frac{L}{b}\right)^2 & b \geq L \\ 0 & b < L \end{cases} \quad (12)$$

resulting in a cumulative distribution:

$$N_{\text{sheet}}(> b; b, L) = \begin{cases} \frac{L}{b} & b \geq L \\ 1 & b < L \end{cases} \quad (13)$$

Thus, the differential distribution expected from sheets is  $\propto b^{-2}$ , and the cumulative distribution is  $\propto b^{-1}$ . The differential distribution is non-zero only at  $b > L$  – and thus is truncated at the sheet-width.

### 3. Comparison with Observational Data

The dependence of the  $b$  distribution  $dN/db \propto b^{-3}$  or  $b^{-2}$  may be present in existing data-sets. In this section, we perform a few comparisons between the data and power-law  $b$ -distributions.

These comparisons may be hampered by contributions to line-measurements of line-blending (when 2 or more individual lines cannot be statistically decomposed, and thus the properties of only one, broader, blended line is measured), and also to the sensitivity of the detection measurement algorithms to lines of these velocity widths. We have assumed that the measurement algorithms are 100% efficient.

We used data from three recently published studies of the Ly $\alpha$  forest absorbers (Hu et al. 1995; Lu et al. 1996; Kirkman & Tytler 1997). From these, we have used only lines with measured column densities  $N_H = 10^{12.5} - 10^{14}$ , and  $b > 35 \text{ km sec}^{-1}$ . Using a KS-test (Press et al. 1995), we determine the probability that data from these observations are consistent with having been drawn from a differential distribution with a single-power-law, for a range of power-law values in 0.05 increments. We tested each data-set individually (datasets 2, 4, and 6, see Table 1), producing 99.5% confidence limits (where the dataset has a 0.5% probability of being drawn from a parent distribution with that power-law value). The results of these are shown in Table 1. The combination of all three datasets (dataset 7) places limits on a single-value-power-law parent population for the differential distribution with a power-law between  $[-4.05, -3.15]$ . The combined data-set is inconsistent with a single-value power-law  $dN/db \propto b^{-3}$  at 99.99% confidence, and inconsistent with  $dN/db \propto b^{-2}$  at  $(100 - 2 \times 10^{-29})\%$  confidence.

In Fig. 2b, there is what looks like an apparent break from a single power-law in the data near  $b = 80 \text{ km sec}^{-1}$ . In a combined dataset from all three observations, using values of  $b > 80 \text{ km sec}^{-1}$ , we find the 99.5% upper-limit on the power-law slope is  $-3.5$  (the lower-limit is  $-11$ ). This is consistent with the range found for  $35 < b < 60 \text{ km sec}^{-1}$  ( $[-4.55, -2.05]$ , 99.5% confidence range, drawn from dataset 7; 346 lines). Thus, the break is not statistically significant.

#### 4. Discussion and Conclusions

We have described a model in which we have assumed the absorbing structures of the Ly $\alpha$  forest may be idealized as infinite sheets and cylinders in velocity space. In this model, the measured LOS velocity width  $b$  is due to the line-of-sight size in velocity space of the absorbing structure, determined both by its physical size in comoving space and by its peculiar velocity structure. Assuming a random orientation of these structures relative to the LOS, a high-velocity-tail to the distribution of LOS velocity widths of the Ly $\alpha$  forest is produced. This tail is due to the chance occurrence of a LOS passing close to the long-axis, making the total traverse distance much longer than that of a LOS which passes nearly perpendicular to the long axis. The differential distribution due to an ensemble of infinite cylinders (sheets) shows a dependence  $N_{\text{cyl}}(> b) \propto b^{-3}$  ( $N_{\text{sheet}}(> b) \propto b^{-2}$ ).

The shape of the  $L$ -distribution (the characteristic size of the structure) will dominate the observational  $b$ -distribution at low values (*i.e.*  $b \approx L$ ). Thus, in this model the Gaussian which is observed in the velocity range  $b \approx 10\text{-}40 \text{ kmsec}^{-1}$  is largely due to the shape of the  $L$  distribution, while the high-velocity tail is due to the line-of-sight penetrating absorbing structures close to their long-axis.

The single power-law differential  $b$ -distribution of  $b^{-3}$  for cylinders and  $b^{-2}$  for sheets should continue up to values of  $b \sim \infty$  only if these structures are infinitely long. This is almost certainly not the case. At high values of  $b$ , the distribution should break from these power-laws, due to the finite size of the absorbing structures.

A comparison with a combined dataset of 447 lines with  $b > 35 \text{ km sec}^{-1}$  places limits on the value of the power-law distribution, with  $dN/dB \propto b^{-[4.05, 3.15]}$  (99.5% confidence limits). A pure power-law  $\propto b^{-3.0}$  is excluded at a probability of  $1 \times 10^{-4}$  while  $\propto b^{-2.0}$  is excluded at  $2 \times 10^{-31}$ . Under this model, including values of  $b$  toward lower velocities ( $b \sim L_{\text{max}}$ ) could bias the power-law toward more negative values; however, using a dataset consisting only of higher velocities ( $b > 80 \text{ km sec}^{-1}$ ) the data are even more inconsistent with  $dN/db \propto b^{-3}$ . Therefore such low- $b$  contamination cannot be responsible for the inconsistency between the

observational data and the predicted power-law dependency. The effects of finite-length sheets and filaments may be responsible for the steepness of this power-law. Further work on the observational limits of such a break could provide a direct measurement of the size of these structures. Hydrodynamic simulations can play an important role in predicting the form and magnitude of this break, providing observers with the tools they need to find it.

In conclusion, modeling the absorbing structures of the IGM responsible for the Ly $\alpha$  forest as infinite cylindrical filaments and sheets in velocity space predicts power-law  $b$ -distributions – which predict more observed high- $b$  lines than are reported in the observations. This can be due to several causes, among them the finite-size of such structures, a decreasing detection efficiency with increasing  $b$ , or that the geometric idealization here presented does not accurately reflect the physical system.

RR acknowledges support through a Max-Planck Fellowship from Max-Planck-Institut für extraterrestrische physik. We are extremely grateful to Lam Hui, for very useful discussions and comments on drafts. This research has made use of the NASA/IPAC Extragalactic Database (NED) which is operated by the Jet Propulsion Laboratory, California Institute of Technology, under contract with the National Aeronautics and Space Administration.



## References

- Bi, H. & Davidsen, A. F., 1997, ApJ **479**, 523+
- Cen, R., Miralda-Escudé, J., Ostriker, J. P., & Rauch, M., 1994, ApJ **437**, L9
- Cen, R. & Simcoe, R. A., 1997, ApJ **483**, 8+
- Duncan, R. C., Vishniac, E. T., & Ostriker, J. P., 1991, ApJ **368**, L1
- Dwight, H. B., 1961, *Tables of Integrals and Other Mathematical Data*, Macmillan, 4th edition
- Hernquist, L., Katz, N., Weinberg, D. H., & Miralda-Escudé, J., 1996, ApJ **457**, L51
- Hu, E. M., Kim, T.-S., Cowie, L. L., Songaila, A., & Rauch, M., 1995, AJ **110**, 1526+
- Hui, L., Gnedin, N. Y., & Zhang, Y., 1997, MNRAS, submitted
- Katz, N., Weinberg, D. H., Hernquist, L., & Miralda-Escudé, J., 1996, ApJ **457**, L57
- Khare, P., Srianand, R., York, D. G., Green, R., Welty, D., Huang, K.-L., & Bechtold, J., 1997, MNRAS **285**, 167
- Kim, T.-S., Hu, E. M., Cowie, L. L., & Songaila, A., 1997, AJ **114**, 1+
- Kirkman, D. & Tytler, D., 1997, ApJ **484**, 672+
- Lu, L., Sargent, W. L. W., Womble, D. S., & Takada-Hidai, M., 1996, ApJ **472**, 509+
- Miralda-Escudé, J., Cen, R., Ostriker, J. P., & Rauch, M., 1996, ApJ **471**, 582+
- Nath, B. B., 1997, ApJ **482**, 621+
- Petitjean, P., Bergeron, J., Carswell, R. F., & Puget, J. L., 1993, MNRAS **260**, 67
- Press, W., Flannery, B., Teukolsky, S., & Vetterling, W., 1995, *Numerical Recipes in C*, Cambridge University Press
- Press, W. H. & Rybicki, G. B., 1993, ApJ **418**, 585+
- Rauch, M., Carswell, R. F., Webb, J. K., & Weymann, R. J., 1993, MNRAS **260**, 589
- Zhang, Y., Anninos, P., & Norman, M. L., 1995, ApJ **453**, L57
- Zhang, Y., Anninos, P., Norman, M. L., & Meiksin, A., 1997, ApJ **485**, 496+

Fig. 1.— Schematic diagram of the absorption. The line-of-sight crosses an absorber with a minimum size  $b_0$  and an infinite length, at an angle  $\theta$  with respect to the perpendicular, producing a total line-of-sight crossing distance of  $b$  km sec $^{-1}$ .

Fig. 2.— Comparison of combined datasets 1+3+5 ( Table 1) with theoretical  $b$ -distribution due to a cylinder with a single radius  $L=28$  km sec $^{-1}$ . **(a)** The differential distribution – the solid histogram is the data, and the broken line is the theoretical prediction, which is a very poor approximation to the data; this indicates that a distribution of cylinder radii is required. **(b)** Integral of the data (and theoretical model) shown in panel (a). It is shown in log-log, to make the power-law nature of both the theoretical distribution and the observed data clear. The apparent break near  $b = 80$  km sec $^{-1}$  in the data is not statistically significant (see Sec. 3).

Table 1.  $b$  Data-sets

Dataset # (ref)	$N_H$ range (cm $^{-2}$ )	$b$ range (km sec $^{-1}$ )	Number of $b$ values	$dN/db \propto b^\alpha$ (99.5% limits)
1(A)	$10^{12.5-14}$	–	328	–
2(A)	$10^{12.5-14}$	>35	116	[–4.1, –2.50]
3(B)	$10^{12.5-14}$	–	790	–
4(B)	$10^{12.5-14}$	>35	252	[–4.55, –3.05]
5(C)	$10^{12.5-14}$	–	287	–
6(C)	$10^{12.5-14}$	>35	84	[–4.70, –2.40]
7(A+B+C)	$10^{12.5-14}$	>35	447	[–4.05, –3.15]
8(A+B+C)	$10^{12.5-14}$	>80	46	< –3.7

References. — (A) Kirkman & Tytler 1997: QSO HS 1946+7658, ( $z=3.02$ )  
(B) Hu et al. 1995: Q0014+813 ( $z=3.38$ ), Q0302-003 ( $z=3.29$ ) 0636+680  
( $z=3.17$ ), 0956+122 ( $z=3.30$ ); (C) Lu et al. 1996: Q0000-26 ( $z=4.1$ )

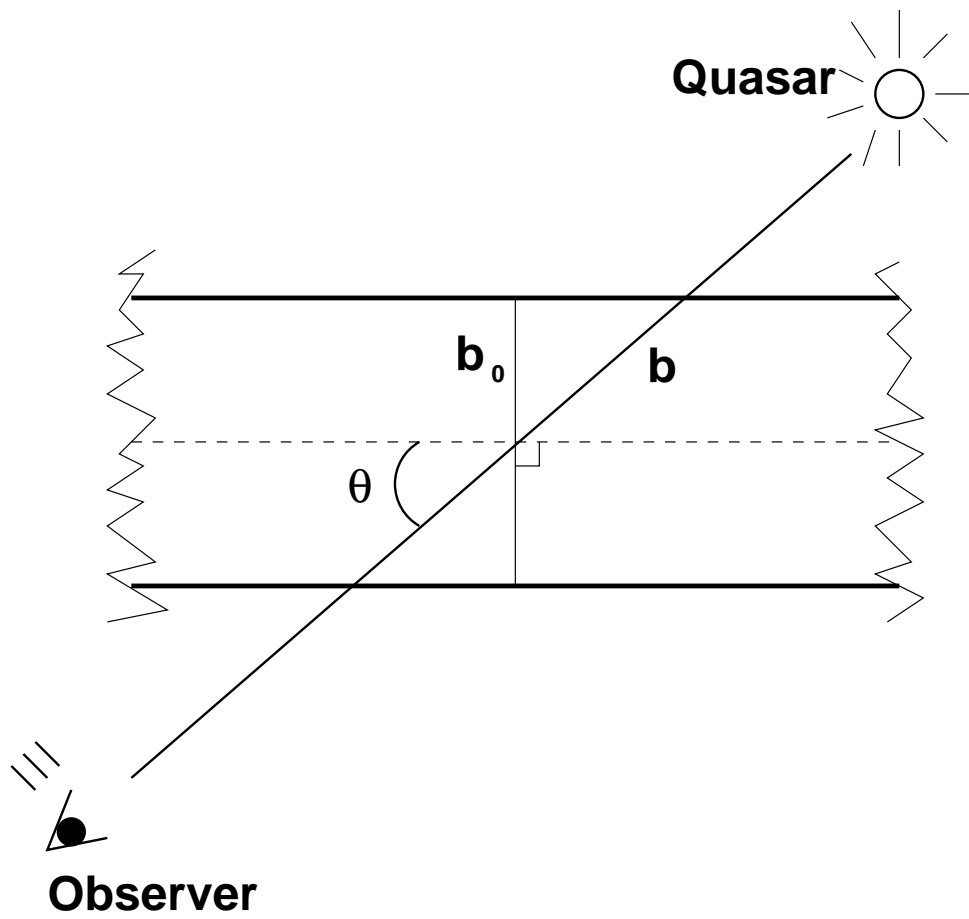


Figure 1

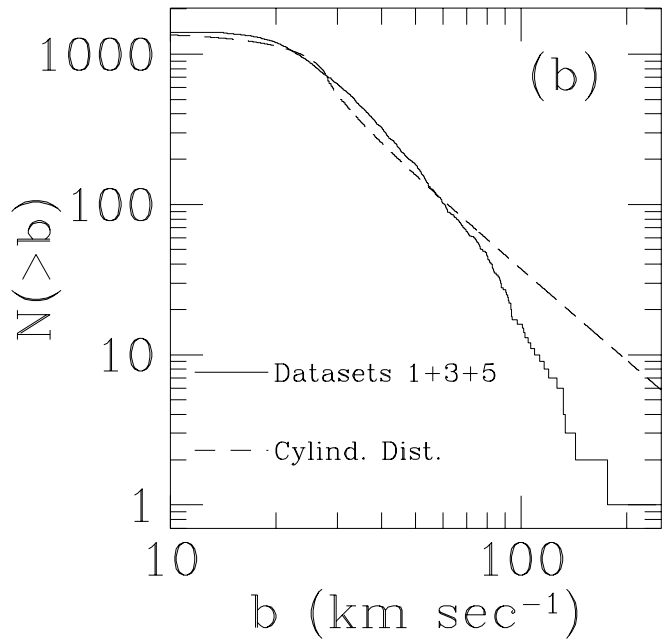
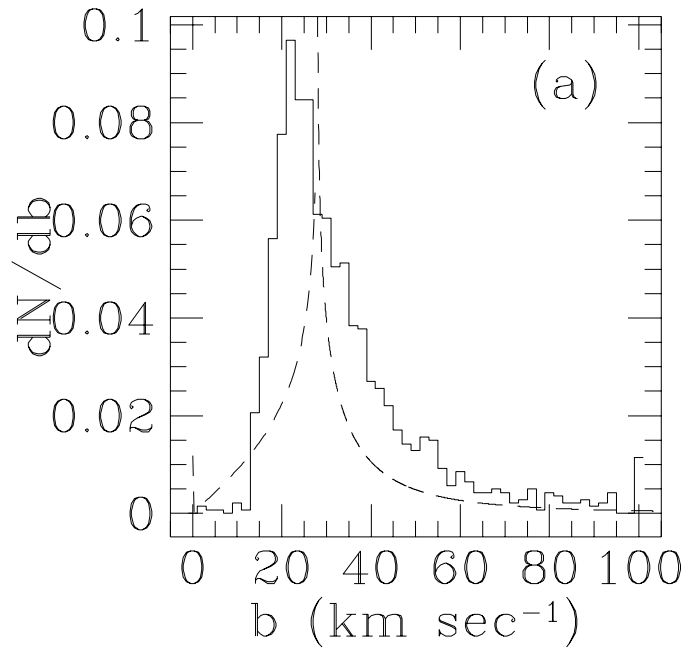


Figure 2